Calibration and validation of a numerical BMI curing model using asymmetric laminated composite plates

Royal NLR - Netherlands Aerospace Centre

Calibration and validation of a numerical BMI curing model using asymmetric laminated composite plates

Problem area

During manufacturing of composite materials residual stress can result in distortion of the final product. In aerospace manufacturing these distortions require the use of shimming during assembly and should therefore be minimized. These distortions are especially critical when building on existing parts, e.g. for a repair, as the added material has to conform to the original structure.

To predict the amount of residual stress and subsequent distortion numerical modelling of the fabrication process can be employed. The model can subsequently be used to inform the mechanic on possible problems with the repair before it is performed. Furthermore, insights can be obtained on how to obtain high quality repairs before any actual work is performed. To this end, an accurate numerical model is required of the employed repair process. A prominent issue when accurately modelling the distortion due to curing is the absence of accurate material parameters. These material parameters can strongly influence the accuracy of the model and are often difficult and costly to obtain experimentally.

Description of work

In this study a numerical model is developed to predict the distortion after curing of RM3000 Bismaleimide (BMI) composite material. Model verification is performed with AS4/8552 material as it is extensively reported in literature. For the RM3000 resin a curing model is developed based on performed Differential Scanning Calorimetry (DSC) measurements. Asymmetric laminates of UD-HTA40/RM3000 composite material are manufactured to obtain experimental results for calibration and validation of the distortion model. 3D scans are made of the asymmetric laminates at different stadia after manufacturing. A method is devised to calibrate unknown thermal expansion coefficients using an experimental procedure. The unknown chemical shrinkage coefficient of

the resin is calibrated in a second step using the calibrated thermal expansion coefficients and the deformation of the asymmetric laminates after manufacturing.

Results and conclusions

The numerical modelling method is verified for reported distortions in literature for AS4/8552 composite material showing good agreement. Subsequently, the cure of the RM3000 resin is successfully modelled and implemented in the numerical model.
The Asymmetric UD-HTA40/RM3000 laminates showed significant deformation directly after manufacturing. From 3D scans of the manufactured UD-HTA40/RM3000 laminates it is observed that the deformation reduces significantly over time, indicating strong relaxation effects.
The calibration experiment for the thermal expansion coefficient was successful, however a range of thermal expansion coefficients was obtained in stead of a single value. To obtain a single value, the range of possible thermal expansion coefficients should be included in the second step of the calibration procedure.
The second step, where the chemical shrinkage and the thermal expansion coefficient are to be calibrated, resulted in non-physical values. It is suspected that this is caused by the relaxation occurring after cure, which is not yet captured in the model. To perform a correct calibration for this resin it is necessary to correctly capture the relaxation effects in the numerical model.

Applicability

The obtained model can be applied to predict deformation and residual stress after manufacturing in composite materials when no significant relaxation occurs in the post cure condition. The calibration procedure to determine the often unknown thermal expansion and chemical shrinkage coefficient can be employed to strongly reduce the experimental work and cost to obtain applicable values. To be able to correctly calibrate the coefficients, the model should be expanded with a relaxation model after curing

GENERAL NOTE
This report is based on a presentation held at the Composites 2021 conference in Gothenburg, 22-24 September 2021.

Calibration and validation of a numerical BMI curing model using asymmetric laminated composite plates

AUTHOR(S):

T.P.A. Koenis	NLR
N. van Hoorn	NLR
W.M. van den Brink	NLR

Royal NLR - Netherlands Aerospace Centre

This report is based on a presentation held at the Composites 2021 conference in Gothenburg, 22-24 September 2021.

The contents of this report may be cited on condition that full credit is given to NLR and the author(s).

This publication has been refereed by the Advisory Committee AEROSPACE VEHICLES.

CUSTOMER	Royal Netherlands Aerospace Centre
CONTRACT NUMBER	-----
OWNER	NLR
DIVISION NLR	Aerospace Vehicles
DISTRIBUTION	Unlimited
CLASSIFICATION OF TITLE	UNCLASSIFIED

APPROVED BY :

AUTHOR							REVIEWER							MANAGING DEPARTMENT						
T.P.A. Koenis							Digitally signed by Ronald Klomp - de Boer Date: 2021.11.23 14:51:54 +01'00'							A.A. ten Dam 2021.11.24 14:41:31 +01'00'						
DATE	2	3	1	1	2	1	DATE							DATE						

Summary

During manufacturing of composite materials residual stresses can result in distortion of the final part. In aerospace manufacturing the use of shimming to accomodate these distortions during assembly should be minimized. This is especially critical when building on existing parts, e.g. for a repair, as the added material has to conform to the original structure. To predict distortions due to curing of thermoset carbon-matrix composites a numerical modelling method is employed. This method includes the cure kinetics, the Cure Hardening Instantaneously Linear Elastic (CHILE) pseudo-viscoelastic model, and the homogenisation of laminae properties employing the Composite Cylinder Assemblage (CCA) model. This method is implemented in ABAQUS by using the USDFLD and EXPAN subroutines. A prominent issue when accurately modelling the distortion due to curing is the absence of accurate material parameters. To this end, a calibration method is proposed to estimate unknown parameters for the numerical curing model (e.g., the thermal expansion and chemical shrinkage coefficients of the resin). The numerical model is calibrated to match the deformation of manufactured specimens with an asymmetrical layup. In addition, the specimens have been reheated, which at the elevated temperature leads to a reduction in deformation. With this approach, the effects of thermal expansion have been isolated from the chemical induced deformation, which facilitates direct calibration of the coefficients of thermal expansion.

Contents

1   Introduction

The use of Carbon Fibre Reinforced Polymer (CFRP) materials in aircraft structures is increasing significantly. Advanced manufacturing capabilities are required to accomplish efficient use of these materials. Numerical process simulation (i.e., virtual manufacturing) can be used to gain more insight in the production process. This can then be applied to minimise the residual stresses that cause deformation of composite parts. Widely known materials (i.e., AS4/8552) have been characterised extensively, which allows for accurate process modelling. For lesser known materials often additional characterisation is required.

Process simulation is a topic that has been extensively researched. Specifically on the composite curing process numerous PhD researches have been conducted. Johnston [1] investigated process-induced deformation for autoclave processing and defined the well-known CHILE approach. Wijskamp, Svanberg, and Garstka [2, 3] investigated process induced distortions to allow for high-precision composite manufacturing. Similarly, Nielson focussed on larger parts for wind turbines [4]. Their approaches show similarities and these methods have been implemented by authors to assess the sensitivities of input parameters [5, 6]. Asymmetric plates are used extensively to show the capabilities of these process induced distortion models [7, 8]. While known materials such as AS4/8552 are fully characterised [9, 10], lesser known materials require characterisation [11, 12]. One example are Bismaleimide (BMI) resins that are used for high temperature applications [13, 14].

The goal of this paper is to predict residual stresses due to curing for repair applications with an HTA40/RM3000 BMI material. In Section 2 the methods and model development is discussed. The initial model is developed for AS4/8552 after which it is modified for HTA40/RM3000. An experimental procedure for calibrating unknown properties is described in Section 3. In Section 4 the results are presented and discussed after which the conclusions are given in Section 5.

2 Model development

2.1 Model development with Hexcel 8552

For the model development it was decided to start with a familiar material to which the performance of the model could be assessed. In literature, AS4/8552 is extensively reported and most, if not all, material properties can be obtained. In this section the cure kinetics, resin stiffness development, and homogenization of elastic and thermal properties is discussed. The procedure is implemented in the USDFLD and EXPAN subroutines in Abaqus.

The cure kinetics are required to predict the degree of cure (α) as a function of process time and temperature (T). Hexcel 8552 has been characterized by NCAMP and is well documented [15]. The cure rate is determined using the following equation,

$$\frac{d\alpha}{dt} = \dot{x} = \left(\frac{1}{\dot{x}_k} - \frac{1}{\dot{x}_d}\right)^{-1},$$

(1)

which has the chemical reaction component defined as,

$$\dot{x}_k = \dot{x}_{k,1} + \dot{x}_{k,2},$$

(2)

where,

$$\dot{x}_{k,i} = k_{0,i} e^{\frac{-E_i}{RT}} (1-\alpha)^{L_i} (\alpha + B_i)^{N_i}.$$

(3)

In addition to the chemical reaction a diffusion component is included,

$$\dot{x}_d = K_d e^{\frac{B}{a(T-T_g)+b}},$$

(4)

where T_g is the glass transition temperature. The glass transition temperature is defined by the Di Benedetto relation as a function of the degree of cure [16].

$$T_g(\alpha) = T_{g0} + \frac{\lambda\alpha(T_{g\infty} - T_{g0})}{1 - \alpha(1-\lambda)}$$

(5)

Here T_{g0} and $T_{g\infty}$ are the glass transition temperatures at zero degree of cure and one degree of cure respectively. These properties can be obtained from DSC measurements. A fitting parameter (λ) is used to define the relation as a function of degree of cure (e.g., $\lambda = 1$ give a linear relation). According to the NCAMP database, Hexcel 8552 has a T_{g0} of 266.15 K, a $T_{g\infty}$ of 523.15 K, and a λ of 0.78. However, during the model development and comparison with literature [9, 10] it was noticed that $T_{g\infty}$ is relatively high, thus it was lowered to 473.15 K. The implementation of the above cure kinetics model is verified by comparison with Zobeiry and Poursartip [10]. An exact match of the glass transition temperature and degree of cure was obtained.

During the curing process the resin transforms from a liquid, to a rubbery like material, and finally to a solid glassy phase. For a correct representation of the resin state an accurate constitutive model is needed. Full viscoelastic models give the closest approximation but require extensive material characterisation [17]. A good alternative is the Cure-Hardening Instantaneously Linear Elastic (CHILE) model by Johnston et al. [1, 10]. Its behaviour is described as follows,

$$E'_m = \begin{cases} E_m^0 & T^* < T_{C1}^* \\ E_m^0 + \frac{T^* - T_{C1}^*}{T_{C2}^* - T_{C1}^*}(E_m^\infty - E_m^0) & \text{for} \quad T_{C1}^* \leq T^* \leq T_{C2}^* \\ E_m^\infty & T^* > T_{C2}^* \end{cases}$$

(6)

where $E_m^0 = 0.0001$, $E_m^\infty = 1$, and $T^* = T_g - T$. For this model there are two calibration parameters T_{C1}^* and T_{C2}^*. Subsequently, the resin modulus (E_m) and Poisson's ratio (ν_m) are determined as follows,

$$E_m = E_{m,R} + E'_m(E_{m,G} - E_{m,R}) \tag{7}$$

$$v_m = v_{m,R} + E'_m(v_{m,G} - v_{m,R}) \tag{8}$$

where the subscripts indicate the rubbery and glassy values listed in Table 1. The rubbery modulus is assumed a factor 1000 lower than the glassy value and the rubbery Poisson's ratio is assumed close to 0.5.

Table 1: General material properties of Hexcel 8552 and Hexply AS4 [18, 19]

Resin parameter	8552	Fibre parameter	AS4
ρ_m [kg/m^3]	1301	ρ_f [kg/m^3]	1790
$E_{m,G}$ [MPa]	4.67E3	E_{f11} [MPa]	228E3
$E_{m,R}$ [MPa]	4.67	$E_{f22,f33}$ [MPa]	15E3
$v_{m,G}$ [-]	0.37	$v_{f12,f13}$ [-]	0.27
$v_{m,R}$ [-]	0.4996	$G_{f12,f13}$ [MPa]	20E3
		G_{f23} [MPa]	5E3

For the material model in Abaqus the resin and fibre properties are homogenised using the Composite Cylinder Assemblage (CCA) model [20, 21]. Details on this procedure are given in Appendix A. As a result the full three-dimensional elastic ply properties can be described as a function of a field variable described in Equation 6. The ply properties determined with the inputs from Table 1, in the rubbery and glassy phases (i.e., zero degree of cure and fully-cured), are given in Table 2. The glassy properties are in the range of properties reported in literature [9, 2]. Note that the out-of-plane properties (i.e., 22 and 33 direction) are equal due to the Uni-Directional (UD) material.

Table 2: AS4/8552 UD ply properties

	Rubbery	Glassy
E_{11} [MPa]	136.80E3	138.68E3
$E_{22/33}$ [MPa]	146.94	9.55E3
$v_{12/13}$ [-]	0.3617	0.2981
v_{23} [-]	0.6996	0.5878
$G_{12/13}$ [MPa]	7.44	5.19E3
G_{23} [MPa]	36.93	3.14E3

The point of gelation is the moment at which cross-linking of polymer chains causes a significant increase in viscosity. At this point the resin transitions from a liquid to a rubbery gel and the material can experience stresses. Through these phases the resin modulus development is described by the CHILE model and the ply stiffness by using the CCA model. At the same time the lamina Coefficient of Thermal Expansion (CTE) and Coefficient of Chemical Shrinkage (CCS) change, depending on the phase. For the CTE a homogenisation similar to the CCA is used, see Appendix A [22]. It is assumed that for a degree of cure below gelation (i.e., viscous liquid resin) all chemical and thermal strains in the matrix are relaxed. As a result, below α_{gel} CCS_m and CTE_m are set to zero. The resin CTE depends on the resin modulus through an identical relation as in Equation 7. A rubbery and glassy resin CTE are defined (i.e., $CTE_{m,R}$ and $CTE_{m,G}$). From the coefficients in Equations 8-11 the thermal and chemical strains increments can be determined.

$$d\varepsilon_{therm,i} = CTE_i \, \Delta T \tag{9}$$

$$d\varepsilon_{chem,i} = CCS_i \frac{d\alpha}{dt} \Delta t \tag{10}$$

In the above equations the fibre longitudinal thermal expansion coefficient ($CTE_{f,11}$), fibre transverse thermal expansion coefficient ($CTE_{f,22}$), resin chemical shrinkage coefficient(CCS_m), and resin thermal expansion coefficients ($CTE_{m,R}$ and $CTE_{m,G}$) can partially be obtained from literature or calibrated based on experiments reported in literature [2].

Table 3: AS4/8552 thermal expansion and chemical shrinkage coefficients

$E_{f,11}$ [1/°C]	-0.4E-6
$E_{f,22}$ [1/°C]	4E-6
S_m	0.006
$E_{m,G}$ [1/°C]	55E-6
$E_{m,R}$ [1/°C]	220E-6

The constitutive model is validated using experimental results obtained by Wijskamp [2]. Wijskamp manufactured 100x10 mm AS4/8552 asymmetrical specimens (i.e., [0_4,90_4]) with a one hold cure-cycle. For the model the resin and fibre properties in Table 1 and Table 2 are used. The thermal expansion coefficient of the fibre in longitudinal direction ($CTE_{f,11}$) has been taken from the datasheet. The chemical shrinkage coefficient (CCS_m) of 0.6% is reported in literature [2]. The other three parameters in Table *3* are calibrated, within a reasonable range, to match the normal stress reported by Wijskamp as illustrated in Figure 1. The resulting AS4/8552 ply CTEs are relatively close to literature, for instance $CTE_{11,G} = 31.29E - 6 \, °C^{-1}$ and $CTE_{22,R} = 116.30E - 6 \, °C^{-1}$ [9]. The CHILE parameters (i.e., $T_{C1}^* = -30 \, °C$ and $T_{C2}^* = 15 \, °C$) have been calibrated to match the characteristic points at 100 and 200 minutes in Figure 1.
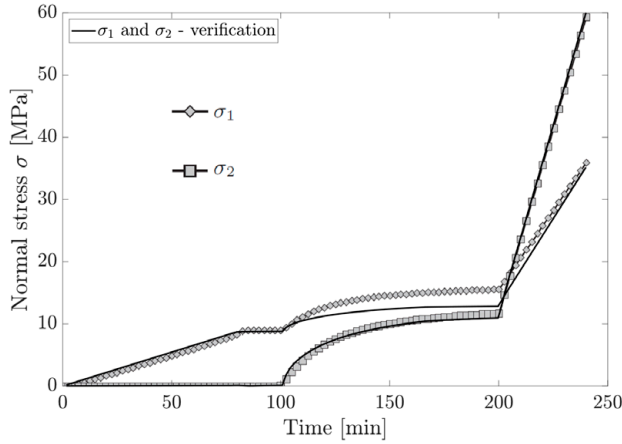

Figure 1: Comparison of the predicted normal stresses with results from Wijskamp [2]
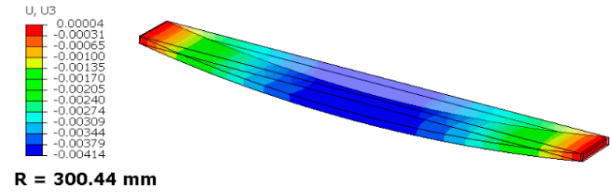
Figure 2: Predicted deformation of a 100x10 mm [0_4,90_4] asymmetrical specimen

It can be seen that the normal stress in 2-direction (i.e., perpendicular to fibres) shows a perfect match. However, despite a good prediction of the final stress, the normal stress in 1-direction does not exactly correspond to Wijskamp's over the full process cycle. It should be noted that the normal stress in 2-direction has the most effect on the resulting curvature. The resulting curvature of a 100x10 mm specimen predicted with our Abaqus model is given in Figure 2. The resulting radius of curvature (3.33 m^{-1}) is close to the model prediction of Wijskamp (3.28 m^{-1}) and within 6% of experimental results (3.14 m^{-1}).

2.2 Model extension to RM3000

As the developed model shows good correlation with literature for AS4/8552 composites, the same approach is used to model the cure process for composites with the BMI-based RM3000 resin. To this end, the model is extended with new material parameters, cure kinetics, and a recalibrated CHILE model. To characterize the RM3000 resin Differential Scanning Calorimeter (DSC) measurements have been performed using a TA instruments Q2000 DSC equipped with a Tzero pan.

Multiple dynamic measurements have been carried out with heat up rates of 1, 2, 5, 10 and 20 °C/min. To describe the cure kinetics of the RM3000 resin system, the autocatalytic Kamal-Sourour model was found to be adequate. The Kamal-Sourour model describes the cure rate as

$$\frac{d\alpha}{dt} = (k_1 + k_2\alpha^m)(1-\alpha)^n \tag{11}$$

with m and n as material constants, α the degree of cure and k_1 and k_2 as rate constants defined as

$$k_i = A_i e^{\left(\frac{-E_i}{RT}\right)} \text{ with } i = 1,2 \tag{12}$$

with A_i the pre-exponential constant, E_i the activation energy, R the universal gas constant and T the absolute temperature [23]. A non-linear regression method in MATLAB is employed to fit the Kamal-Sourour model parameters, A_i, E_i, m and n to the obtained experimental DSC data. To improve the fitting procedure, an initial guess for A_i and E_i is given based on the method by Kissinger [24]. The calibrated parameters and a comparison between the cure-kinetics model and the experimental data is shown in Figure 3 (a). From the same dynamic DSC measurements, both T_{g0} and $T_{g\infty}$ are obtained to use in the Di Benedetto relation of Equation 5 with values of 15.7 °C and 210 °C respectively. The Di Benedetto fitting parameter λ is set to a value of 0.5, as initial sensitivity analysis showed that the influence of this parameter on the deformation after cure is limited.

To obtain the degree of cure at gelation (α_{gel}), isothermal DSC experiments have been performed at temperatures of 200, 220, and 240 °C. The method proposed by Gao et al. is employed to determine the degree of cure at gelation from the isothermal DSC measurements [11]. The reduced reaction rate is extracted from the isothermal DSC data, defined for the Kamal-Sourour fit as

$$V_r = \frac{d\alpha/dt}{(1-\alpha)^n} \tag{13}$$

where the value for the reaction order, n, is set to 1.77. Figure 3 (b) illustrates the reduced reaction rates over the degree of cure for the three isothermal measurements. In this graph the inflection point indicates a change in reaction mechanism corresponding to the gelation of the resin, thus indicating α_{gel}. The inflection point is estimated based on the time derivative of the reduced reaction rate where a value of approximately 0.77 was obtained.
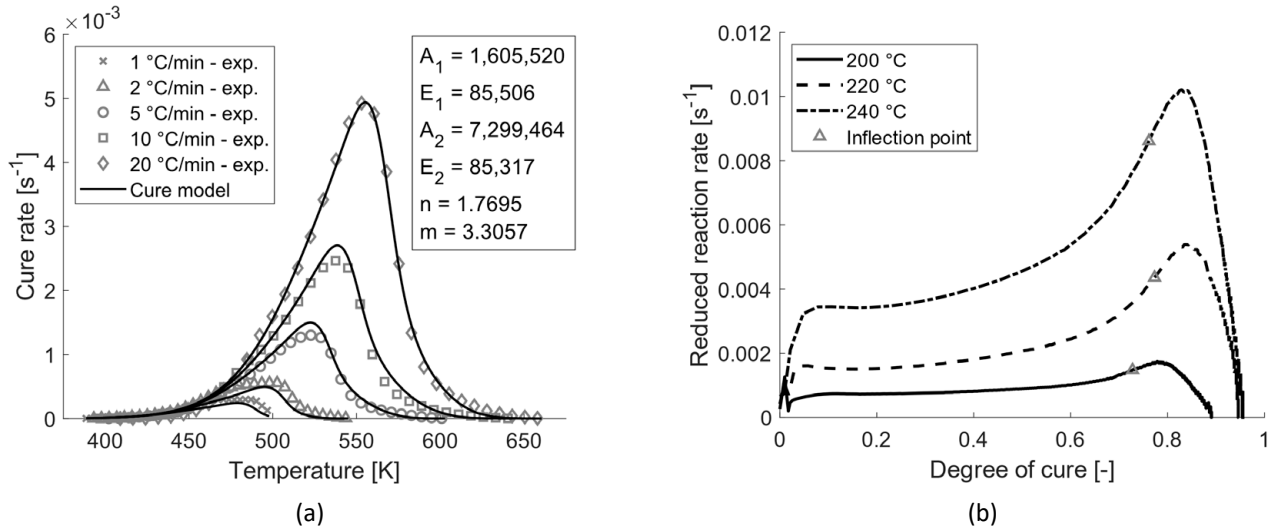
Figure 3: a) comparison of the experimental results with the cure kinetics model for dynamic DSC measurements and b) reduced reaction rate obtained from isothermal DSC measurements with the inflection points indicating gelation

In Section 2.1 the CHILE parameters (i.e., T_{C1}^* and T_{C2}^*) were calibrated for AS4/8552 based on two characteristic transition points. At the first point the resin transitions to a rubbery like material (i.e., resin gelation) where the viscosity starts to increase significantly. The second point aligns with vitrification where the resin becomes glassy. During the production of the asymmetric plates an Optimold sensor was included that measures the degree of cure (i.e., resistance value), as demonstrated in Pantelelis et al. [25]. The CHILE parameters were calibrated to match characteristic points in the cure development, see Figure 4. As a result, $T_{C1}^* = -55\,°C$ and $T_{C2}^* = 55\,°C$. The first point matches a degree of cure equal to gelation. It is observed that this point corresponds to the steepest resistance increase, which additionally verifies that an α_{gel} of 0.77 is valid. The second and third characteristic point are calibrated using T_{C2}^*.
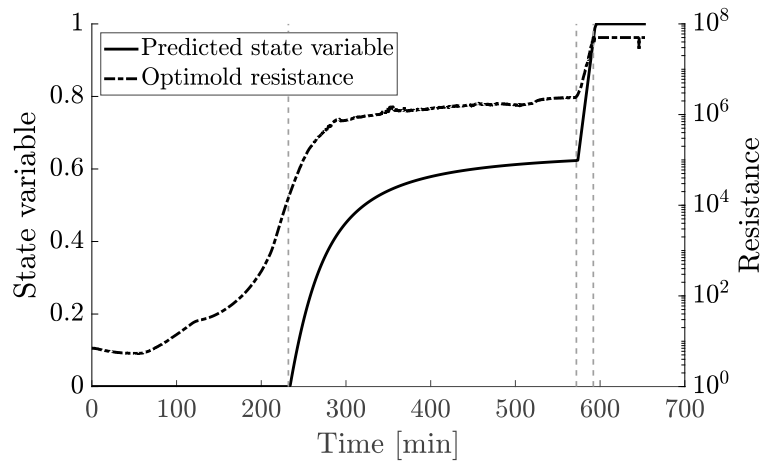

Figure 4: Calibrated CHILE parameters for RM3000 by matching characteristic points of an Optimold cure sensor

2.3   Finite element model

A basic Finite Element (FE) model is generated that incorporates the subroutines mentioned in Section 2.1. First, the cure kinetics were implemented in a HETVAL subroutine for a thermal simulation. It was observed that the resulting temperature differences were minimal due to limited heat development in such thin specimens. Therefore, a homogeneous temperature identical to the applied cure cycle was assumed. Secondly, a model for the CTE calibration step was generated. Each ply is modelled separately with quadratic C3D20 elements, which are necessary to correctly represent the high distortions. After a mesh convergence study a mesh size of 5 mm was found to be sufficient. The ply CTE's are implemented without a subroutine. One non-linear geometry step with a temperature decrease from the stress-free temperature to room temperature is implemented. At last, the model is extended for the full process simulation. Now the expansion is defined using the USDFLD and EXPAN subroutines and two steps are modelled. The first step describes the distortion during cure in which the specimen is fully constrained (i.e., analogous to the vacuum bag). In a second step this constraint is released and the specimen is free to deform as illustrated in Figure 2.

3 Methods

3.1 Specimen Manufacturing and Materials

In this study asymmetrical laminates of UD-HTA40/RM3000 have been manufactured using vacuum assisted resin transfer moulding (VARTM) similarly as in Evsyukov et al. [26]. The laminates with original dimensions of 210x25 mm are trimmed to dimensions of 200x20 mm to limit effects of inconsistent edges. The layup of the four laminates is displayed in Table 5, where the fibre volume fraction of laminates 9040 and 9041 is 0.57 and 9042 and 9043 is 0.625. The temperature during resin infusion was set to 117 °C. After the infusion, the temperature is increased with 0.5 °C/min to 147 °C, followed by a 1h dwell, followed by a ramp of 0.5 °C/min to 193 °C and a dwell of 6h. After this cure cycle, the specimens are cooled to room temperature with a cooling rate of 2 °C/min. After manufacturing the laminates deform due to the asymmetrical lay-up, resulting in a different curvature for each layup [7, 8]. The curvature of the laminates has been measured directly after curing as well as after trimming using a 3D scanner. These deformations are used to calibrate and validate the developed numerical model.

For the modelling of the cure process of UD-HTA40/RM3000 laminates, most elastic material parameters are readily available from data sheets as displayed in Table 4. However, values for the thermal expansion and chemical shrinkage coefficients of the resin are inconclusive or not available in literature, even though they have a significant impact in the deformation after manufacturing.

Table 4: Elastic material properties of the RM3000 resin and the HTA40 UD fibres [27, 28]

Resin parameter	RM3000	Fibre parameter	HTA40
ρ_m [kg/m^3]	1 250	ρ_f [kg/m^3]	1 760
$E_{m,G}$ [MPa]	3.2e3	E_{11} [MPa]	238e3
$E_{m,R}$ [MPa]	3.52	$E_{22,33}$ [MPa]	15e3
$v_{m,G}$ [-]	0.365	$v_{12,13}$ [-]	0.3
$v_{m,R}$ [-]	0. 4996	v_{23} [-]	0.3
$G_{m,G}$ [MPa]	1.17e3	$G_{12,13}$ [MPa]	25
$G_{m,R}$ [MPa]	1.17	G_{23} [MPa]	7

3.2 Calibration procedure

To obtain representative values for the thermal expansion and chemical shrinkage coefficients, a calibration procedure has been developed. This procedure consists of multiple experimental and numerical stages to decouple effects of chemical shrinkage and thermal expansion to facilitate direct calibration of the thermal expansion coefficients.

To isolate the thermoelastic strain of the asymmetric plates, an experiment is performed where the manufactured laminates are reheated. Two of the trimmed laminates have received a DIC pattern, and have been subsequently fixed in a temperature controlled oven. The asymmetric plates have been fixed by clamping an aluminium rod which has been glued to the back of the laminates using temperature resistant silicone glue. Figure 5 shows the set-up as used for this experiment. The oven is heated in steps of 15 °C from room temperature to 155 °C. At each temperature step, the deformation of the plates is captured using stereoscopic DIC. To allow for a clear view for the cameras, the oven is opened for a short period of time for each measurement. The temperature of the specimens is measured by K-type thermocouples fit to the back of the laminates. From the stereoscopic DIC images, a 3D model of the asymmetric

laminate is obtained in .stl format. The curvature is extracted with a custom MATLAB routine, where it is assumed that the laminate deform in a circular shape. By assuming a linear relation between the curvature and the laminate temperature, the stress free temperature (T_{sf}), the temperature where the laminate has 0 curvature, is computed from the curvature measurements [7]. The T_{sf} should be higher than the cure temperature, as both the process induced thermoelastic strain and non-thermoelastic strain are to be counteracted by the reheating of the laminate [27].
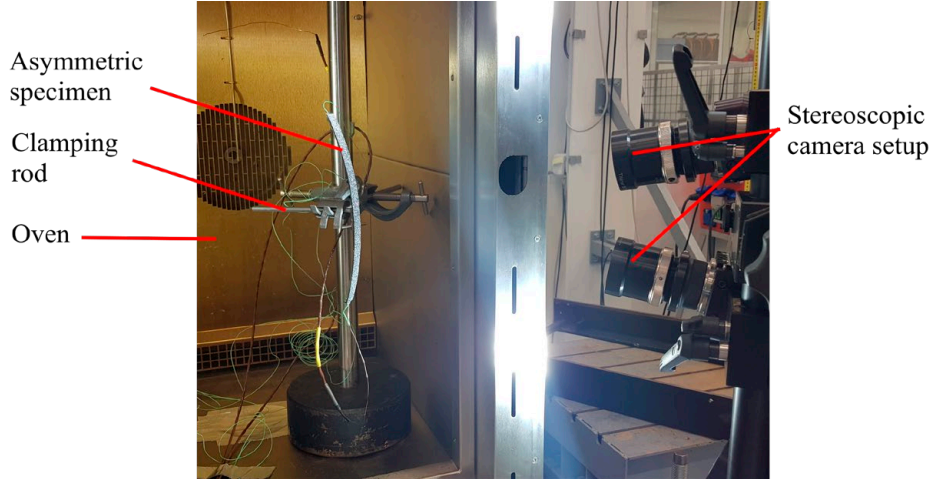

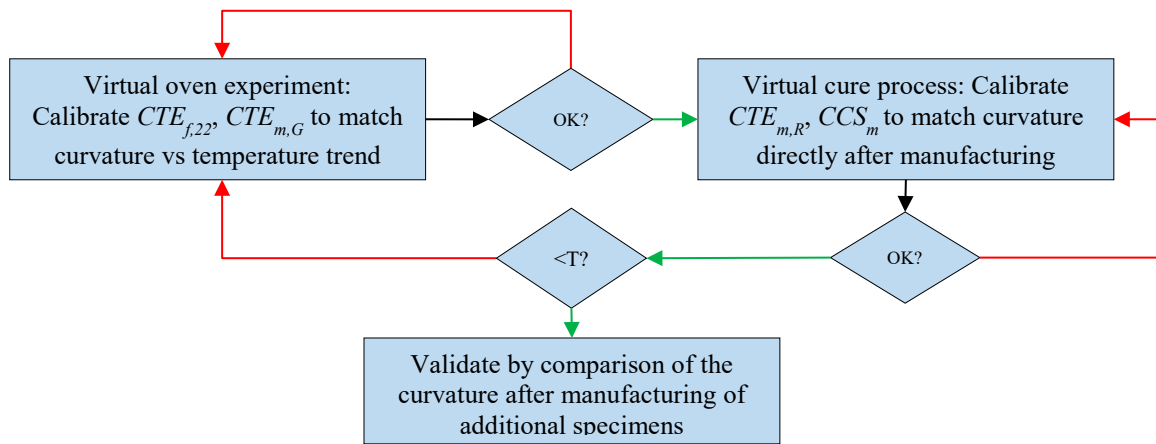Figure 5: Experimental set-up to capture the laminate curvature at elevated temperatures

Figure 6: Schematic illustration of the intended numerical calibration steps to calibrate the thermal expansion and chemical shrinkage coefficients

Figure 6 illustrates the intended numerical calibration procedure. First, a numerical model is developed of the oven experiment for both tested laminates to calibrate the thermal expansion coefficients of the fibre and the resin in the glassy state. The FE model consists of the HTA40/RM3000 laminate which starts in a stress free, fully cured, and flat state at T_{sf} as determined experimentally. The temperature in the simulation is lowered from T_{sf} to the room temperature, which results in deformation purely due to thermoelastic strain. Linear spaced ranges of 11 steps for $CTE_{f,22}$ and $CTE_{m,G}$ ranging from 0 to 3E-5 and 1E-5 to 6E-5 respectively are used to run 121 simulations per laminate to match the slope of the curvature over temperature relation. The value for $CTE_{f,11}$ is given by the datasheet, and is thus not varied [28]. For this calibration, it is assumed that the plate is fully cured, and no non-thermoelastic strains influence the curvature in the reheating experiment.

The calibrated values for $CTE_{f,22}$ and $CTE_{m,G}$ are used in the second stage of the numerical calibration. In this stage, the numerical model developed in this study is employed to model the cure process of the asymmetric laminates to calibrate the $CTE_{m,R}$ and the CCS_m of the resin. By varying these parameters, the numerically obtained curvature after manufacturing is matched with the experimentally obtained curvature.

4   Results & Discussion

4.1   Calibration experiment

The curvature of the four manufactured laminates has been extracted from 3D scans taken directly after manufacturing and after trimming of the laminates. The measured curvatures of both stages are displayed in Table 5, showing very limited effect of the trimming of the edges.

Table 5: Layup and curvatures of the manufactured asymmetrical laminates

Laminate nr.	Layup	Curvature after cure [m^{-1}]	Curvature after trimming [m^{-1}]	Curvature start re-heating exp. [m^{-1}]
9040	[(60,-60)$_2$,30,-30,30]	3.18	3.15	2.78
9041	[60,-60,60,-60,30,-60]	2.41	2.34	-
9042	[90,0,90$_6$]	3.81	3.78	3.35
9043	[90,0$_4$]	1.02	1.22	-

Laminates 9040 and 9042 are used in the reheating experiment as they show the highest curvature. Figure 7 (a) and (b) illustrate the curvatures of laminates 9040 and 9042 at different temperatures. A linear relation is observed between the curvature and the temperature which corresponds with findings of Gigliotti et al. [7]. This indicates no further chemical shrinkage occurs during the reheating of the specimens. Linear lines have been fitted to the data by least-squares regression, and the stress free temperature (T_{sf}) is extracted as indicated in Figure 7.
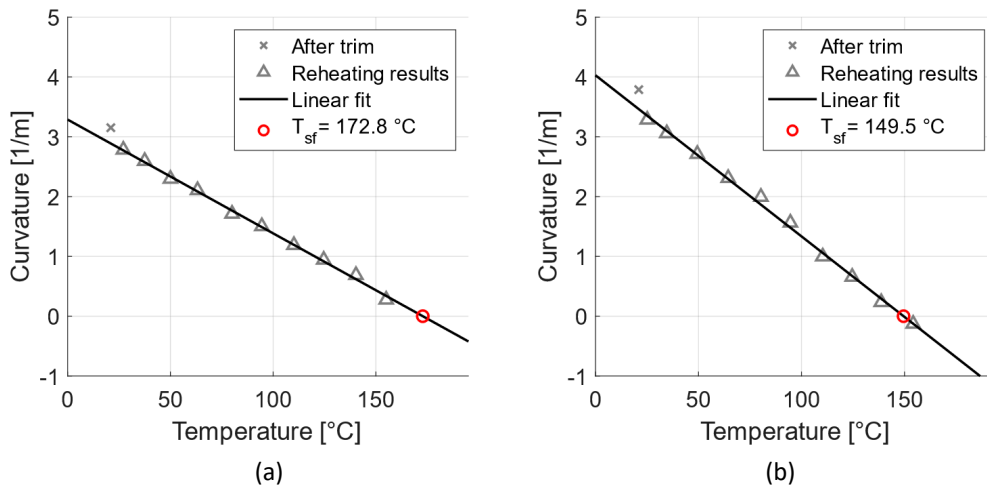

Figure 7: Curvature over temperature for specimens (a) 9040 and (b) 9042 with the linear trend and stress free temperature

The T_{sf} of the laminates is significantly lower than the cure temperature of 193 °C. This indicates that in the time between the moment of manufacturing and the moment of reheating (42 days) relaxation of the process induced residual stresses has occurred. Relaxation of the residual stresses reduce the curvature of the laminates, lowering the T_{sf}. This is substantiated when comparing the curvature after trimming with the curvature at the start of the reheating experiment. As shown in Table 5, the curvature has reduced by over 11 % for both the 9040 and 9042 laminate in the period between trimming and the reheating experiment. Moreover, when shifting the linear relation to match the curvature after trimming, indicated by the cross in Figures 9 (a) and (b), the stress free temperature is still significantly

lower than expected. It is suspected that the laminates have experienced significant relaxation between the moment of cure and the moment the 3D scans are taken. Despite relaxation, the results of this experiment can still be used in the numerical calibration, as the linear curvature-temperature relation has been captured. However, it should be investigated if the slope of this linear relation is influenced by the reduction in curvature at room temperature due to the possible stress relaxation. If this is the case, more extensive iteration would be required to take into account the residual stresses after cure in the CTE calibration.

4.2   Thermal expansion Calibration

The CTE calibration simulations have been performed both for laminate 9040 and 9042 for all combinations of $CTE_{f,22}$ and CTE_m, as described in Section 3.2. Per simulation result, the curvatures at 100 °C and at room temperature are extracted to determine the slope of the curvature over temperature relation. The obtained slope is compared with the experimentally determined slope for laminates 9040 and 9042 to determine the error of the simulation. The error for both laminates is combined to obtain a total error, as illustrated in Figure 8. A line of minimum error is obtained by linear interpolation for both laminates, indicated by the dashed line in Figure 8. As the minimum error line for both laminates are almost parallel, no single optimum value is obtained for the $CTE_{f,22}$ and $CTE_{m,G}$ when the errors are combined. Instead, a combined minimum error line is obtained, where the minimum error is defined as the combination that results in the lowest error for both laminates. As the CTE calibration experiment does not result in a single optimum, it is decided to deviate from the intended procedure of Section 3.2 and include the minimum error combinations of $CTE_{m,G}$ and $CTE_{f,22}$ in the second calibration step for the calibration of the chemical shrinkage.
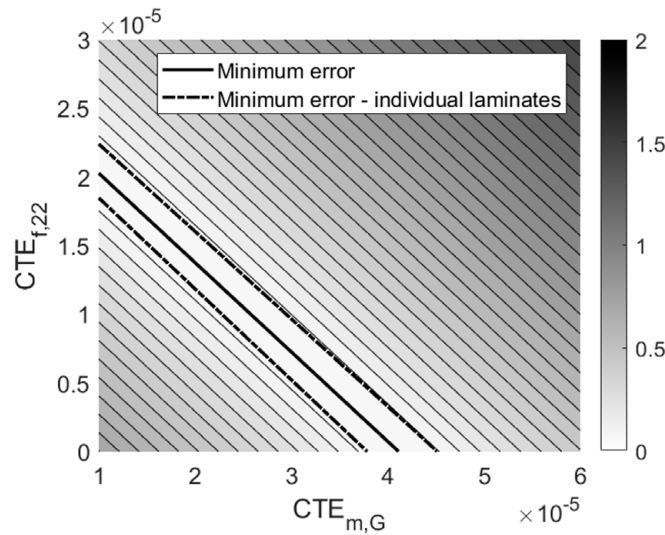

Figure 8: Contour plot of the error between numerical and experimental results of the thermal calibration experiment combining results for the 9040 and 9042 laminates.

The minimum error line as indicated in Figure 8 is only slightly dependent on the use of different curvatures at room temperature. Therefore, the results as presented are sufficient to continue with the next step in the calibration procedure.

4.3   Chemical shrinkage calibration

Similarly to the CTE calibration, the CCS calibration simulations have been performed both for laminate 9040 and 9042 in trimmed state, for a range of CCSm and the minimum error combinations of $CTE_{m,G}/CTE_{f,22}$. The amount of curvature after cure is not significantly influenced by the value used for $CTE_{m,R}$. Therefore, its value is fixed at three times the value for $CTE_{m,G}$. The range for $CTE_{m,G}$ is moved to span the values on the minimum error line of Figure 8. The numerical results have been compared to the experimental curvatures.
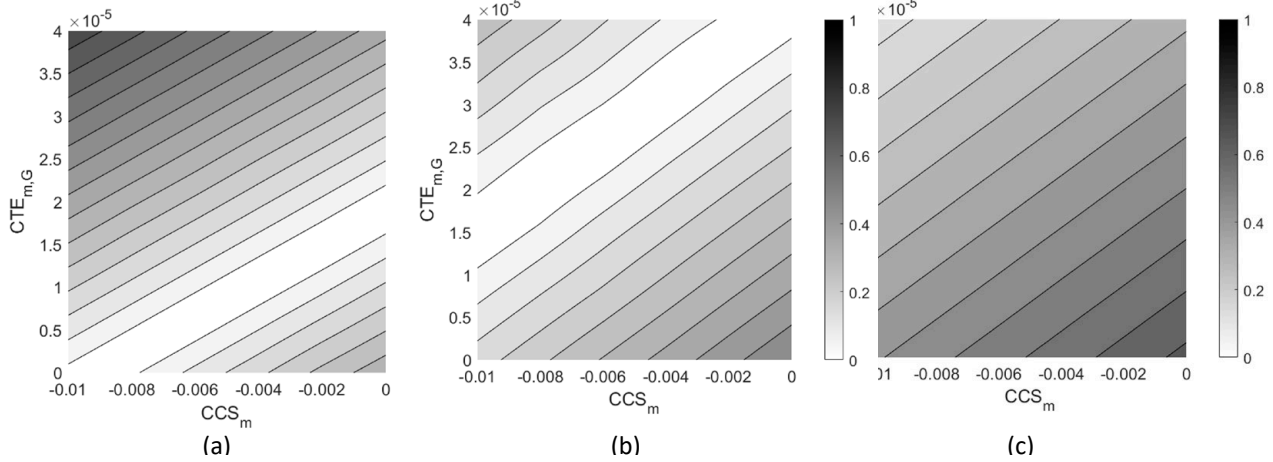

Figure 9: Contour plots of the error in laminate curvature for the numerical model employing a range of values for in CCS_m and $CTE_{m,G}$ ordered from most to least deformed laminate (a) 9042, (b) 9040 and (c) 9041

Figure 9 (a) and (b) display the linearly interpolated error contour plots of laminates 9042 and 9040 respectively. Similarly to the CTE calibration, a minimum error line for both laminates can be obtained. By extrapolating the minimum error lines a cross-over point is reached with a minimum error. However, this cross-over point is located in the region of a negative thermal expansion coefficient. Furthermore, for conventional values of $CTE_{m,G}$ (> 30E-6) the numerical simulation of laminate 9042 would require a positive value for CCS_m which is also non-physical.

It is theorized that due to relaxation of the residual stresses during and after manufacturing the curvature measurements are significantly lower than can be predicted with the current model. This is substantiated by the observations of the stress free temperature as discussed in Section 4.1. In contrast to similar studies, such as performed by Kravchenko et al. [8], the laminates manufactured in this study are forced flat during the cure cycle and for multiple hours thereafter before they are released. This additional stress induced by forcing the laminates in a flat shape could strongly influence the amount of relaxation occurring during and just after manufacturing.

If the employed model captured all phenomena present in the VARTM cure process, the minimum error lines should all cross in a region with realistic values for CCS_m and $CTE_{m,G}$. It is speculated that the amount of relaxation depends on the amount of residual stress induced by the cure process, therefore shifting the minimum error differently per laminate. The same CCS calibration procedure has been performed for laminate 9041, which showed less deformation after manufacturing than both laminate 9040 and 9042. The error contour for this laminate is displayed in Figure 9 (c). As the subfigures of Figure 9 are ordered by decreasing curvature after manufacturing, it is visible how for larger process induced residual stresses, the minimum error line shifts down. From these observations it is theorized that by including relaxation in the numerical model, the minimum error lines of the different laminates could be shifted, and a single value for the calibration parameters can be obtained.

5   Conclusions

The developed numerical model for AS4/8552 composites has been validated, where good agreement with literature has been observed. The relatively simple CHILE model was found accurate enough for this application. A Kamal-Sourour curing model for the BMI resin RM3000 has been fit to dynamic DSC measurements showing good results. In the asymmetric HTA40/RM3000 laminates the distortion due to thermal expansion has successfully been isolated from chemical effects by reheating of manufactured HTA40/RM3000 laminates. However, numerical calibration of these parameters result in an infinite amount of combinations of $CTE_{f,22}$ and $CTE_{m,G}$ that result in the minimum error. Therefore, one of these parameters should be included in the calibration of the chemical shrinkage coefficient.

Optimal values for CCS_m and $CTE_{m,G}$ have not been found in the second step of the calibration, as the developed model does not sufficiently describe relaxation occurring during and after the curing process.

6 Acknowledgements

7 References

[1] A. A. Johnston, An integrated model of the development of process-induced deformation in autoclave processing of composite structures, Vanvouver: The University of British Columbia, 1997.

[2] S. Wijskamp, Shape distortions in composites forming, Enschede: Universiteit Twente, 2005.

[3] T. Garstka, Separation of process induced distortions in curved composite laminates, Bristol: University of Bristol, 2005.

[4] M. W. Nielsen, Prediction of process induced shape distortions and residual stresses in large fibre reinforced composite laminates, Copenhagen: Technical University of Denmark, 2012.

[5] K. VanClooster, J. Gilbert, F. Pascon and L. V. Stepan, "Predicting the Influence of Manufacturing Parameters on Curing Generated Deformations Using Thermo-mechanical Modelling," in *American Society for Composites*, Seattle, 2018.

[6] V. Chabridon, "Robust Probabilistic Analyses of Composite Part Manufacturing," National Aerospace Laboratory NLR, Amsterdam, 2014.

[7] M. Gigliotti, M. R. Wisnom and K. D. Potter, "Development of curvature during the cure of AS4/8552 [0/90] unsymmetric composite plates," *Composites Science and Technology,* vol. 63, pp. 187-197, 2003.

[8] O. G. Kravchenko, S. G. Kravchenko and R. B. Pipes, "Cure history dependence of residual deformation in a thermosetting laminate," *Composites: Part A,* vol. 99, pp. 186-197, 2017.

[9] N. Ersoy, T. Grastka, K. Potter, M. R. Wisnom, D. Porter, M. Clegg and G. Stringer, "Development of the properties of a carbon fibre reinforced thermosetting composite through cure," *Composites: Part A,* vol. 41, pp. 401-409, 2010.

[10] N. Zobeiry and A. Poursartip, "The origins of residual stress and its evaluation in composite materials," *Structural Interity and Durability of Advanced Composites,* pp. 43-72, 2015.

[11] J. Gao, L. Li, Y. Deng, Z. Gao, C. Xu and Z. Mingxi, "Study of gelation using Differential Scanning Calorimetry (DSC)," *Journal of Thermal Analysis,* vol. 49, pp. 303-310, 1997.

[12] E. Kappel, "An engineering approach for Prepreg characterization," *Composites Part C,* vol. 4, p. 100083, 2021.

[13] R. Srinivasan, T. J. Wang and L. J. Lee, "Chemorheology of high temerature rtm resins," in *ANTEC 95*, Boston, 1995.

[14] A. Khattab, Exploratory development of VARIM process for manufacturing high temperature polymer matrix, Missouri: University of Missouri, 2005.

[15] A. Shahkarami, D. Van Ee and A. Poursartip, *Material Characterization for Processing: Hexcel 8552,* NCAMP, National Center for Advanced Materials Performance, 2009.

[16] G. Struzziero, B. Remy and A. A. Skordos, "Measurement of thermal conductivity of epoxy resins during cure," *Journal of Applied Polymer science,* vol. 136, p. 47015, 2019.

[17] J. M. Svanberg, Predictions of Manufacturing Induced Shape Distortions, Luleå: Luleå University of Technology, 2002.

[18] Hexcel®, *HexPly® 8552, Product Data Sheet FTA-072-AG16,* 2016.

[19] Hexcel®, *HexTow® AS4, Product Data Sheet CTA 311 JA20,* 2020.

[20] C. C. Chamis, *NASA Tech. Memo 8329,* 1983.

[21] C. C. Chamis, F. Abdi, M. Garg, L. Minnetyan, H. Baid, D. Huang, J. Housner and F. Talagani, "Micromechanics-based progressive failure analysis prediction for WWFE-III composite coupon test cases," *Journal of Composite Materials,* vol. 47, no. 20, pp. 2695-2712, 2013.

[22] D. A. Hopkins and C. C. Chamis, "A Unique Set of MicromechanicsEquations for High-Temperature Metal Matrix Composites," in *Testing Technology of Metal Matrix Composites, ASTM STP 964*, Philadelphia, 1988.

[23] M. R. Kamal and S. Sourour, "Kinetics and thermal characterization of thermoset cure," *Polym Eng Sci,*

vol. 13, pp. 59-64, 1973.

[24] H. E. Kissinger, "Variation of Peak Temperature With Heating Rate in Differential Thermal Analysis," *Journal of Research of the National Bureau of Standards,* vol. 57, pp. 217-221, 1956.

[25] N. Pantelelis, E. Bistekos, W. Gerrits, S. Wilkens, D. Breen and S. Wilson, "Non-intrusive intelligent cure monitoring for enhancing the manufacturing of high-temp composite structures," in *SAMPE Europe Conference 2021*, Baden/Zürich, 2021.

[26] S. Evsyukov, R. Klomp-de Boer, H. Stenzenberger, T. Pohlmann and M. ter Wiel, "A new m-xylylene bismaleimide-based high performance resin for vacuum assisted infusion and resin transfer molding," *Journal of Composite Materials,* vol. 53, no. 22, pp. 3062-3072, 2019.

[27] M. Abouhamzeh, J. Sinke and R. Benedictus, "Investigation of curing effects on distortion of fibre metal laminates," *Composite Structures,* vol. 122, pp. 546-552, 2015.

[28] Toho Tenax Europe GmbH, *Delivery programme and characteristics for Tenax® HTA filament yarn,* 2011.

[29] Z. Hashin, "Analysis of Composite Materials - A Survey," *Journal of Applied Mechanics,* vol. 50, no. 3, pp. 481-505, 1983.

[30] B. W. Rosen and Z. Hashin, "Effective thermal expansion coefficients and specific heats of composite materials," *International Journal of Engineering Science,* vol. 8, no. 2, pp. 157-173, 1970.

[31] Renegade Materials Corporation, "RM-3000 Bismaleimide (BMI) Resin Transfer Molding (RTM) Resin," Product Data Sheet, 2018.

[32] S. Wijskamp, R. Akkerman and E. A. D. Lamers, "Residual stresses in non-symmetrical carbon/epoxy laminates," in *International conference on composites: bridging the gap between academia and industrie*, ICCM 14. California: San Diego, 2003.

Appendix A

The CCA model assumes a 2D representation of the UD fibre composite [29], which is used to determine the ply properties from the fibre and matrix properties. The matrix material is assumed isotropic such that the shear modulus can be determined as

$$G_m = \frac{E_m}{2(v_m+1)} \tag{14}$$

The ply transverse bulk modulus (k) can be calculated from the fibre volume fraction (V_f), G_m, and the fibre and matrix transverse bulk moduli. The matrix volume fraction (V_m) equals 1-V_f.

$$k = \frac{k_m(k_f+G_m)V_m+k_f(k_m+G_m)V_f}{(k_f+G_m)V_m+(k_m+G_m)V_f} \tag{15}$$

$$\frac{1}{k_f} = -\frac{1}{G_{f23}} - \frac{4v_{f12}^2}{E_{f11}} + \frac{4}{E_{f22}} \qquad\qquad \frac{1}{k_m} = -\frac{1}{G_m} - \frac{4v_m^2}{E_m} + \frac{4}{E_m}$$

From this the ply longitudinal modulus (E_{11}), in-plane Poisson's ratio (v_{12}), and in-plane shear modulus (G_{12}) can be determined. Also, $v_{13} = v_{12}$ and $G_{13} = G_{12}$.

$$E_{11} = E_{f11}V_f + E_mV_m + \frac{4(v_{f12}-v_m)V_f}{\frac{V_m}{k_f}+\frac{V_f}{k_m}+\frac{1}{G_m}} \tag{16}$$

$$v_{12} = v_{f12}V_f + v_mV_m + \frac{4(v_{f12}-v_m)\left(\frac{1}{k_m}-\frac{1}{k_f}\right)V_mV_f}{\frac{V_m}{k_f}+\frac{V_f}{k_m}+\frac{1}{G_m}} \tag{17}$$

$$G_{12} = \frac{G_m[G_mV_m+G_{f12}(1+V_f)]}{G_m(1+V_f)+G_{f12}V_m} \tag{18}$$

For the out-of-plane properties and transverse modulus (E_{22}) an upper and lower bound is calculated. The lower and upper bound of the out-of-plane shear modulus (G_{23}) are,

$$G_{23-} = G_m + \frac{V_f}{\frac{1}{G_{f23}-G_m}+\frac{(k_m+2G_m)V_m}{2G_m(k_m+G_m)}} \tag{19}$$

$$G_{23+} = \frac{G_m[1+(1+\beta_1)V_f]}{\vartheta-V_f\left(1+\frac{3\beta_1^2(1-V_f)^2}{\alpha V_f^3+\psi}\right)} \tag{20}$$

where $\psi = 1$ if $G_{f23} > G_m$ and $k_f > k_m$, otherwise $\psi = -\beta_1$, and,

$$\beta_1 = \frac{k_m}{k_m+2G_m} \qquad \beta_2 = \frac{k_f}{k_m+2G_{f23}} \qquad \gamma = \frac{G_{f23}}{G_m} \qquad \vartheta = \frac{\gamma+\beta_1}{\gamma-1} \qquad \alpha = \frac{\beta_1-\gamma\beta_2}{1+\gamma\beta_2}$$

The upper and lower bound of the transverse moduli (E_{22} and E_{33}) are,

$$E_{22\pm} = E_{33\pm} = \frac{4}{\frac{1}{G_{23\pm}}+\frac{1}{k}+\frac{4v_{12}^2}{E_{11}}} \tag{21}$$

from which the bounds of the out-of-plane Poisson's ratio ($v_{23\pm}$) are determined as [20],

$$v_{23\pm} = V_f\left(\frac{E_{f22}}{2G_{f23}} - 1\right) + V_m\left(2v_m - \frac{E_{22\pm}}{E_{11}}v_{12}\right) \tag{22}$$

For homogenising the fibre and matrix CTE's a similar procedure is used from Rosen and Hashin [30].

$$CTE_{11} = \frac{CTE_{f,11}E_{f11}V_f + CTE_m E_m V_m}{E_{f11}V_f + E_m V_m} \tag{23}$$

$$CTE_{22/33} = CTE_{f,22}\sqrt{V_f} + CTE_m\left(1 - \sqrt{V_m}\right)\left(1 + \frac{V_f V_m E_{f11}}{E_{f11}V_f + E_m V_m}\right) \tag{24}$$

Here V_f is the fibre volume fraction and V_m the matrix volume fraction (i.e., $1 - V_f$). In addition to the thermal effects the resin shrinks due to the chemical reactions during curing. Therefore, the chemical shrinkage has to be described. For the ply CCS a rule of mixtures is used as defined below [2].

$$CCS_{11} = \frac{CCS_m E_m V_m}{E_{f11}V_f + E_m V_m} \tag{25}$$

$$CCS_{22/33} = CCS_m\left[(1 + \nu_m)V_m - \frac{E_m V_m(V_f \nu_{f12} + V_m \nu_m)}{E_{f11}V_f + E_m V_m}\right] \tag{26}$$

Royal NLR - Netherlands Aerospace Centre

NLR operates as an objective and independent research centre, working with its partners towards a better world tomorrow. As part of that, NLR offers innovative solutions and technical expertise, creating a strong competitive position for the commercial sector.

NLR has been a centre of expertise for over a century now, with a deep-seated desire to keep innovating. It is an organisation that works to achieve sustainable, safe, efficient and effective aerospace operations.

The combination of in-depth insights into customers' needs, multidisciplinary expertise and state-of-the-art research facilities makes rapid innovation possible. Both domestically and abroad, NLR plays a pivotal role between science, the commercial sector and governmental authorities, bridging the gap between fundamental research and practical applications. Additionally, NLR is one of the large technological institutes (GTIs) that have been collaborating over a decade in the Netherlands on applied research united in the TO2 federation.

From its main offices in Amsterdam and Marknesse plus two satellite offices, NLR helps to create a safe and sustainable society. It works with partners on numerous programmes in both civil aviation and defence, including work on complex composite structures for commercial aircraft and on goal-oriented use of the F-35 fighter. Additionally, NLR helps to achieve both Dutch and European goals and climate objectives in line with the Luchtvaartnota (Aviation Policy Document), the European Green Deal and Flightpath 2050, and by participating in programs such as Clean Sky and SESAR.

For more information visit: **www.nlr.org**